

Prion protein attenuates excitotoxicity by inhibiting NMDA receptors

Houman Khosravani, Yunfeng Zhang, Shigeki Tsutsui, Shahid Hameed, Christophe Altier, Jawed Hamid, Lina Chen, Michelle Villemaire, Zenobia Ali, Frank R. Jirik, and Gerald W. Zamponi

Vol. 181 No. 3, May 5, 2008. Pages 551–565.

In Fig. 2 D, the rise times for NMDA receptor-mediated miniature synaptic currents were plotted incorrectly. The correct values for the mean mEPSC rise time from baseline to peak should be 7.3 ± 0.3 ms and 8.5 ± 0.1 ms for WT and KO cultures, respectively. The interpretations of our overall findings and the conclusions presented in our original manuscript are not affected by this correction.

Prion protein attenuates excitotoxicity by inhibiting NMDA receptors

Houman Khosravani,¹ Yunfeng Zhang,¹ Shigeki Tsutsui,² Shahid Hameed,¹ Christophe Altier,¹ Jawed Hamid,¹ Lina Chen,¹ Michelle Villemaire,² Zenobia Ali,² Frank R. Jirik,² and Gerald W. Zamponi¹

¹Department of Physiology and Biophysics, Hotchkiss Brain Institute, and ²Department of Biochemistry and Molecular Biology, McCaig Institute for Bone and Joint Health, University of Calgary, Calgary T2N4N1, Canada

It is well established that misfolded forms of cellular prion protein ($\text{PrP}[\text{PrP}^C]$) are crucial in the genesis and progression of transmissible spongiform encephalitis, whereas the function of native PrP^C remains incompletely understood. To determine the physiological role of PrP^C , we examine the neurophysiological properties of hippocampal neurons isolated from PrP -null mice. We show that PrP -null mouse neurons exhibit enhanced and drastically prolonged N -methyl-D-aspartate (NMDA)-evoked

currents as a result of a functional upregulation of NMDA receptors (NMDARs) containing NR2D subunits. These effects are phenocopied by RNA interference and are rescued upon the overexpression of exogenous PrP^C . The enhanced NMDAR activity results in an increase in neuronal excitability as well as enhanced glutamate excitotoxicity both *in vitro* and *in vivo*. Thus, native PrP^C mediates an important neuroprotective role by virtue of its ability to inhibit NR2D subunits.

Introduction

Prions are proteinaceous infectious agents that were first discovered because of their role in the etiology of transmissible spongiform encephalopathies (TSEs), a set of fatal neurological disorders that include human Creutzfeldt-Jakob disease, ovine scrapie, and bovine spongiform encephalitis (Prusiner et al., 1998; DeArmond and Prusiner, 2003). TSEs arise from progressive misfolding of the endogenous cellular prion protein ($\text{PrP}[\text{PrP}^C]$) into disease-associated scrapie form (PrP^{Sc}), which, in turn, disrupts normal cellular function and results in the formation of aggregates and amyloid-like plaques (DeArmond, 2004). Although there has been a clear association between PrP^{Sc} with these disease states, the cellular function of PrP^C remains incompletely understood (Brown, 2001). PrP^C is expressed across the entire central nervous system and at particularly high levels in the hippocampus, striatum, and frontal cortex, with apparently wide subcellular distribution, including synaptic sites (Sales et al., 1998; Fournier et al., 2000). A synaptic role of PrP^C is consistent with evidence from PrP -null mice showing deficits in spatial learning (Criado et al., 2005), altered long-term potentiation

(Collinge et al., 1994; Manson et al., 1995; Curtis et al., 2003; Maglio et al., 2004, 2006), and increased excitability of hippocampal neurons (Colling et al., 1996, 1997; Collinge et al., 1994; Mallucci et al., 2002). Several studies have also suggested that PrP^C may provide neuroprotection. For example, cultured hippocampal neurons obtained from PrP -null mice show an increased apoptosis during oxidative stress (Vassallo and Herms, 2003). Mice lacking PrP^C show increased neuronal damage after ischemic stroke, whereas protection is evident upon the viral-based overexpression of PrP^C in rats (McLennan et al., 2004; Shyu et al., 2005; Spudich et al., 2005; Weise et al., 2006). Finally, in several *in vivo* models of seizure activity, PrP -null mice showed increased mortality, likely as a consequence of hyperexcitability leading to excitotoxicity (Walz et al., 1999). However, the cellular and molecular basis for these effects remains unknown.

Neuronal excitability and excitotoxic neuronal cell death are also features associated with N -methyl-D-aspartate (NMDA) receptor (NMDAR) activity (Mody and MacDonald, 1995; Arundine and Tymianski, 2004). These receptors are comprised of two obligatory NR1 subunits that coassemble with two NR2 subunits into a tetrameric channel complex that is activated by glutamate and is permeable to both sodium and calcium ions. Four different NR2 subunit genes are expressed in the mammalian brain, and it is thought that neonatal synapses are mainly comprised of NR1/NR2B receptors, whereas adult synapses preferentially express NR2A-containing receptors (Cull-Candy and Leszkiewicz, 2004).

Correspondence to Gerald W. Zamponi: zamponi@ucalgary.ca

Abbreviations used in this paper: αCSF, artificial cerebrospinal fluid; APV, aminophosphonovaleic acid; DIV, day *in vitro*; fEPSP, field excitatory postsynaptic potential; GABA, γ-aminobutyric acid; mEPSC, miniature excitatory postsynaptic current; mIPSC, miniature inhibitory postsynaptic current; NMDA, N -methyl-D-aspartate; NMDAR, NMDA receptor; PrP, prion protein; TSE, transmissible spongiform encephalopathy; TTX, tetrodotoxin; WT, wild type.

The online version of this article contains supplemental material.

NR2D receptor subunits are intriguing because their functionality has not been demonstrated in native synaptic currents, although they appear to be present at the protein level (Misra et al., 2000; Thompson et al., 2002). The NR2 subunit isoform is a key determinant of the functional properties of NMDARs, such as activation, desensitization, and deactivation kinetics, with NR2D subunits showing dramatically slower kinetic properties compared with other NR2 (e.g., NR2B) subtypes when expressed heterologously (Cull-Candy and Leszkiewicz, 2004). Receptors containing different types of NR2 subunits share voltage-dependent block by magnesium ions, coactivation by glycine, and inhibition by organic molecules such as MK-801 and amino-phosphonovaleric acid (APV). In this context, it is interesting to note that the elevated susceptibility to neuronal damage observed in the PrP-null mice is diminished by the NMDAR blocker MK-801 (Rangel et al., 2007), suggesting the possibility that PrP^C may perhaps act by regulating NMDAR function.

In this study, we show that the absence of PrP^C gives rise to the appearance of synaptic NMDAR currents with increased amplitude and slowed kinetics that resemble those of NR2D-containing receptors, thus implying enhanced NMDAR activity in PrP-null neurons. Consistent with this finding, *in vitro* and *in vivo* excitotoxicity assays reveal increased neuronal cell death in PrP-null cultures and animals upon transient exposure to NMDA. We demonstrate a novel functional role for PrP^C as a modulator of synaptic NMDA currents and also attribute a neuroprotective function to this molecule by way of its ability to suppress NMDAR activity.

Results

PrP-null mice exhibit greater basal excitability

To examine a possible role of PrP^C in neuronal excitability, we compared synaptic physiology in horizontal hippocampal slices obtained from adult (postnatal day [P] 30–45) wild-type (WT) and PrP-null ($\text{PrP}^{-/-}$) mice. Paired-pulse stimulation of Schaffer collaterals evoked paired synaptic responses in CA1 neurons when bathed in artificial cerebrospinal fluid (aCSF). In WT slices, the synaptic responses observed were typical of hippocampal slice physiology, with waveforms exhibiting a robust presynaptic volley, a sharp downward deflecting population spike, and upward deflecting field excitatory postsynaptic potential (fEPSP) as well as robust paired-pulse facilitation (Fig. 1 A). Paired evoked field potentials in slices from PrP-null mice exhibited similar waveform properties and similar paired-pulse facilitation but showed an increase in the number of overriding polyspikes (Fig. 1, A and B). This suggests that neurons in PrP-null slices fire multiple action potentials in response to a single stimulus and indicates a basal increase in excitability. The minimum stimulus threshold required to evoke a single population spike was reduced in PrP-null slices (Fig. 1 C, top), as was the stimulus intensity required to reach maximum response (Fig. 1 C, middle). In contrast, the magnitude of paired-pulse facilitation did not differ between WT and PrP-null mouse slices (Fig. 1 C, bottom). The increased apparent excitability of the null mouse neurons was abolished at room temperature, which is consistent

with previous findings under similar conditions (Lledo et al., 1996). In PrP-null slices, bath application of 50 μM APV attenuated or abolished the occurrence of overriding population spikes, resulting in waveforms that were similar to recordings from WT slices (Fig. 1 D). These data indicate that the enhanced excitability observed in the PrP-null mice is in large part caused by the activity of NMDARs. In contrast, treatment with 100 μM of the γ -aminobutyric acid (GABA_A) receptor blocker picrotoxin did not reduce the number of population spikes in the PrP-null slices (reported for pulse 2: $\text{PrP}^{+/+}$, 1.2 ± 0.2 spikes, $n = 5$; $\text{PrP}^{-/-}$, 3.0 ± 0.44 spikes, $n = 5$; $P = 0.006$).

Removal of Mg²⁺ ions from the extracellular medium is known to induce a hyperexcitable state mainly as a result of the unblocking of NMDARs. To determine whether the absence of PrP^C protein exacerbates this effect, we compared the effect of removing extracellular Mg²⁺ ions on slices from WT and PrP-null mice. Brain slice recordings were initially performed in normal aCSF to confirm the presence of stable field potentials. Slices were then exposed to an external solution containing zero Mg²⁺ (ZM-aCSF), and evoked synaptic responses were assessed using paired-pulse stimuli (Fig. 1 E). Slices from both WT and PrP-null mice exhibited hyperexcitability within 5 min after exposure to ZM-aCSF and exhibited a marked increase in the number of population spikes, which was exacerbated in the PrP-null mice (Fig. 1 F, left). Prolonged perfusion with ZM-aCSF is known to result in the appearance of epileptiform discharges that progress to seizurelike events in a subset of the slices. Under ZM conditions, the time to the appearance of the first discharge was significantly shortened for PrP-null slices (Fig. 1 F, second graph). Furthermore, in slices that progressed to seizure-like activity, the time to onset was significantly reduced, whereas the seizure duration was unaffected (Fig. 1 F, third and fourth graphs). Fourier transform analysis of the discharges revealed greater high frequency content in the discharges recorded in PrP-null slices compared with those obtained from WT animals, which is consistent with increased excitability in PrP-null slices (Fig. S1, available at <http://www.jcb.org/cgi/content/full/jcb.200711002/DC1>). Collectively, these data are consistent with the results obtained in normal aCSF and indicate that augmentation of NMDARs by Mg²⁺ unblock exacerbates the effects of PrP^C on neuronal excitability.

Alterations in synaptic NMDAR-mediated currents in PrP-null mice

To directly measure the effect of PrP^C on synaptic NMDAR currents, we recorded miniature excitatory postsynaptic currents (mEPSCs) in mature (12–16 d *in vitro* [DIV]) primary hippocampal cultures bathed in ZM-aCSF supplemented with tetrodotoxin (TTX), picrotoxin, CNQX, and glycine. As shown in Fig. 2, mEPSCs recorded from PrP-null neurons showed events with significantly larger amplitudes than those observed in WT slices (Fig. 2, A–D). Furthermore, NMDAR-mediated mEPSCs of PrP-null mouse neurons exhibited significantly longer decay times (Fig. 2, B–D). In contrast, the frequency of events and rise time of the mEPSCs were unaffected by the absence of PrP^C. Significant changes were also observed in some parameters associated with AMPA/kainate-mediated mEPSCs and in

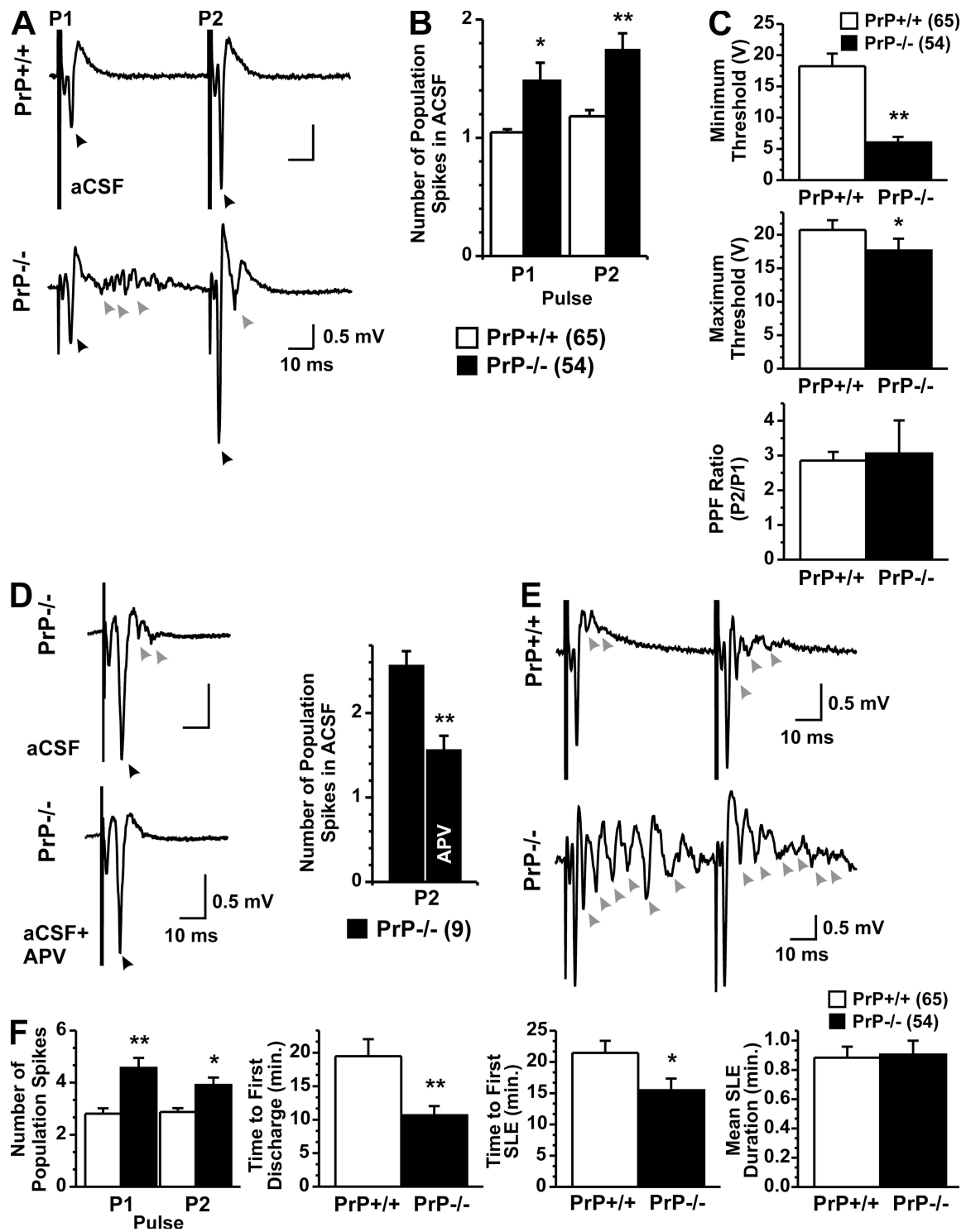


Figure 1. Field potentials recorded in the CA1 layer of hippocampal slices from WT and PrP-null mice. (A) Paired pulses evoked by stimulation of the Schaffer collaterals in slices from P30–45 mice in normal artificial cerebrospinal fluid (aCSF). (B) Quantification of the number of population spikes in WT and PrP-null slices in aCSF. (C, top) Minimum stimulus intensity required to evoke a single population spike in WT and PrP-null slices. (middle) Stimulus intensity required to evoke maximum single population spike amplitude. (bottom) Extent of paired pulse facilitation in WT and PrP-null slices. (D, top) Field potentials recorded from PrP-null slices before and after the application of 50 μ M APV as shown for P2. (bottom) Quantification of the number of population spikes before and after APV application in PrP-null slices. (E) Evoked field potentials recorded after 5 min of perfusion in zero-magnesium aCSF (ZM-aCSF). The gray arrows indicate successive population spikes, which are augmented in the PrP-null slices. (F, left) The number of population spikes overriding the fEPSP in slices exposed to ZM-aCSF. (second graph) Time to the observance of the first seizurelike discharge in ZM-aCSF. (third graph) Time to the occurrence of the first seizurelike event (SLE) upon perfusion with ZM-aCSF. (right) Duration of seizurelike events in WT and PrP-null slices. The black and gray arrowheads indicate the primary population spikes and the additional population spikes, respectively, overriding the fEPSP in each pulse (P1 and P2); these latter polyspikes were only observed in PrP-null mice. Data are represented as mean \pm SEM (error bars) with statistical significance denoted as *, P < 0.05 and **, P < 0.001. Numbers in parentheses indicate the number of slices.

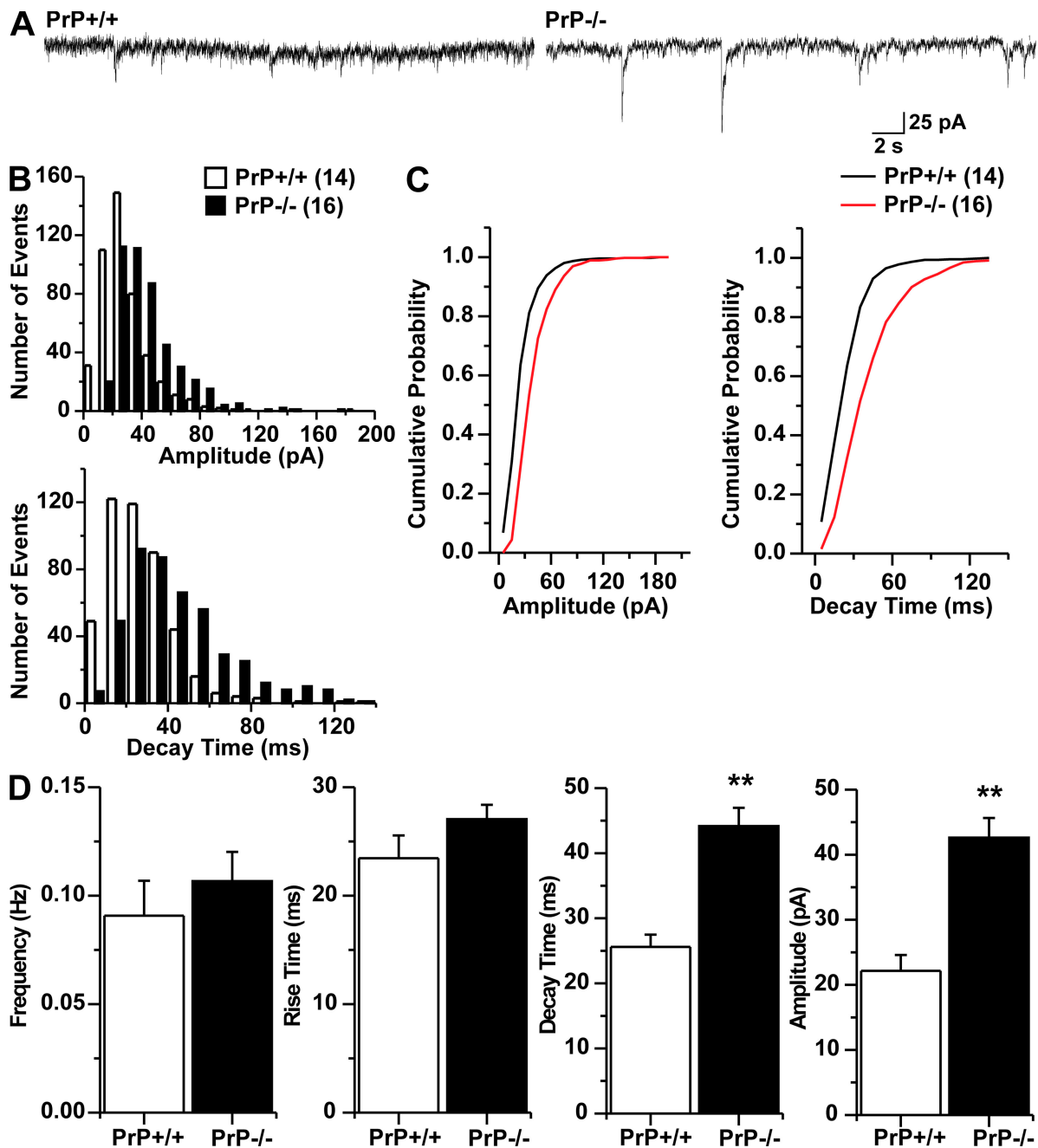


Figure 2. Analysis of miniature synaptic NMDAR currents in cultured hippocampal neurons from WT and PrP-null mice. (A) Representative examples of raw mEPSCs recorded in mature (12–16 DIV) WT and PrP-null hippocampal neurons in culture. In PrP-null neurons, NMDA-mediated mEPSCs were observed to be larger and showed prolonged decay times. (B) Event histograms for mEPSC amplitude (top) and decay time (bottom). Note that mEPSCs in PrP-null neurons exhibit a shift toward larger amplitude events and increased decay time constants. (C) Cumulative probability plots for mEPSC amplitude and decay time showing a shift in each summed distribution toward larger events with longer decay times ($P < 0.05$; Kolmogorov-Smirnov test). (D) Mean values for mEPSC waveform parameters showing increased EPSC amplitudes and prolonged decay times. Here, decay time refers to the time required for an e-fold reduction in peak current amplitude. Data are represented as mean \pm SEM (error bars), with statistical significance denoted as *, $P < 0.05$ and **, $P < 0.001$. Numbers in parentheses indicate the number of cells.

GABA_A-mediated miniature inhibitory postsynaptic current (mIPSCs), but these effects were smaller in magnitude than those observed with NMDAR-mediated events (Fig. S2, available at <http://www.jcb.org/cgi/content/full/jcb.200711002/DC1>). Overall, these data are consistent with the increased excitability observed in PrP slices and, furthermore, provide direct evidence of PrP^C-mediated modulation of synaptic NMDARs.

To conduct a more detailed analysis of NMDAR-mediated currents, NMDARs were activated by transient and focal application of NMDA puffs to cultured hippocampal neurons held under voltage clamp. Currents were evoked using different puff durations from a glass patch pipette filled with 100 μ M NMDA in the presence of TTX, picrotoxin, CNQX, and glycine. As shown in Fig. 3, NMDA currents recorded from PrP-null mice

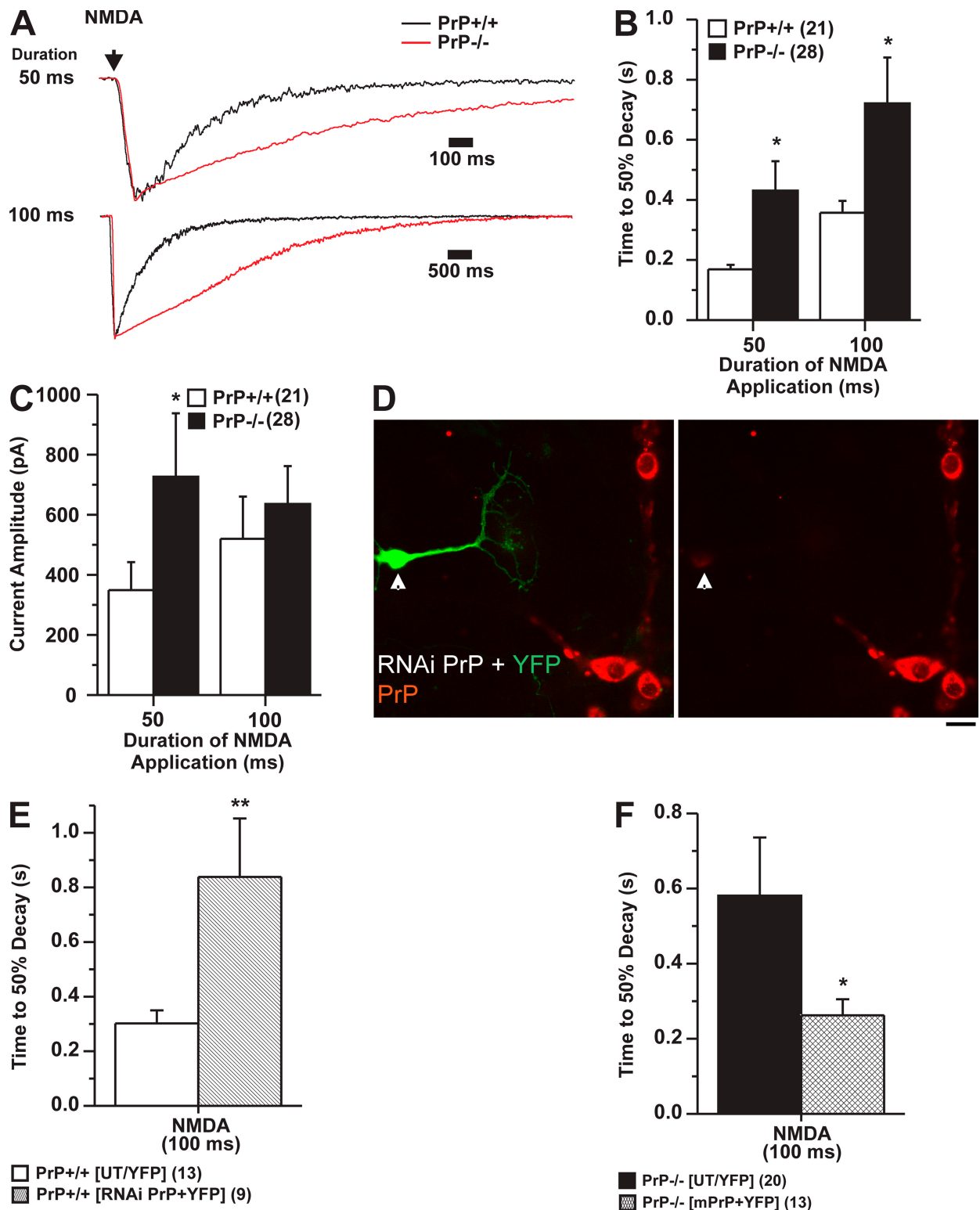


Figure 3. Kinetic analysis of evoked NMDAR-mediated currents in cultured hippocampal neurons from WT and PrP-null mice. (A) Representative NMDAR-mediated currents in response to 100- μ M transient NMDA puff application at 50- and 100-ms durations for WT (black) and PrP-null (red) neurons. Note the prolonged decay kinetics in the PrP-null neurons. The records were arbitrarily scaled to overlap at peak. (B) Time to 50% decay (i.e., the time required for decay to half-maximum peak current amplitude) for WT and PrP-null neurons. (C) Current amplitudes evoked by 50- and 100-ms puffs of NMDA for WT and PrP-null neurons. (D, left) Cultured WT mouse hippocampal neurons cotransfected with YFP and siRNA against PrP^C and permeabilized and stained with a PrP^C antibody. Note that the YFP-positive (i.e., siRNA transfected) cell is negative for PrP^C, whereas a YFP-negative cell in the same dish shows robust PrP expression. The arrowheads indicate the location of the soma. (E) Time to 50% decay for WT neurons transfected with siRNA against PrP for an NMDA puff duration of 100 ms. Data were compared with culture-matched neurons transfected with YFP alone or nearby untransfected (UT) cells within the same siRNA-transfected culture. (F) Time to 50% decay for PrP-null neurons transfected with PrP cDNA plus a YFP marker. Currents were evoked with a 100-ms puff of NMDA. Data were compared with culture-matched YFP alone or untransfected cells. Data are represented as mean \pm SEM (error bars), with statistical significance denoted as *, P < 0.05 and **, P < 0.001. Numbers in parentheses indicate the number of cells. Bar, 30 μ m.

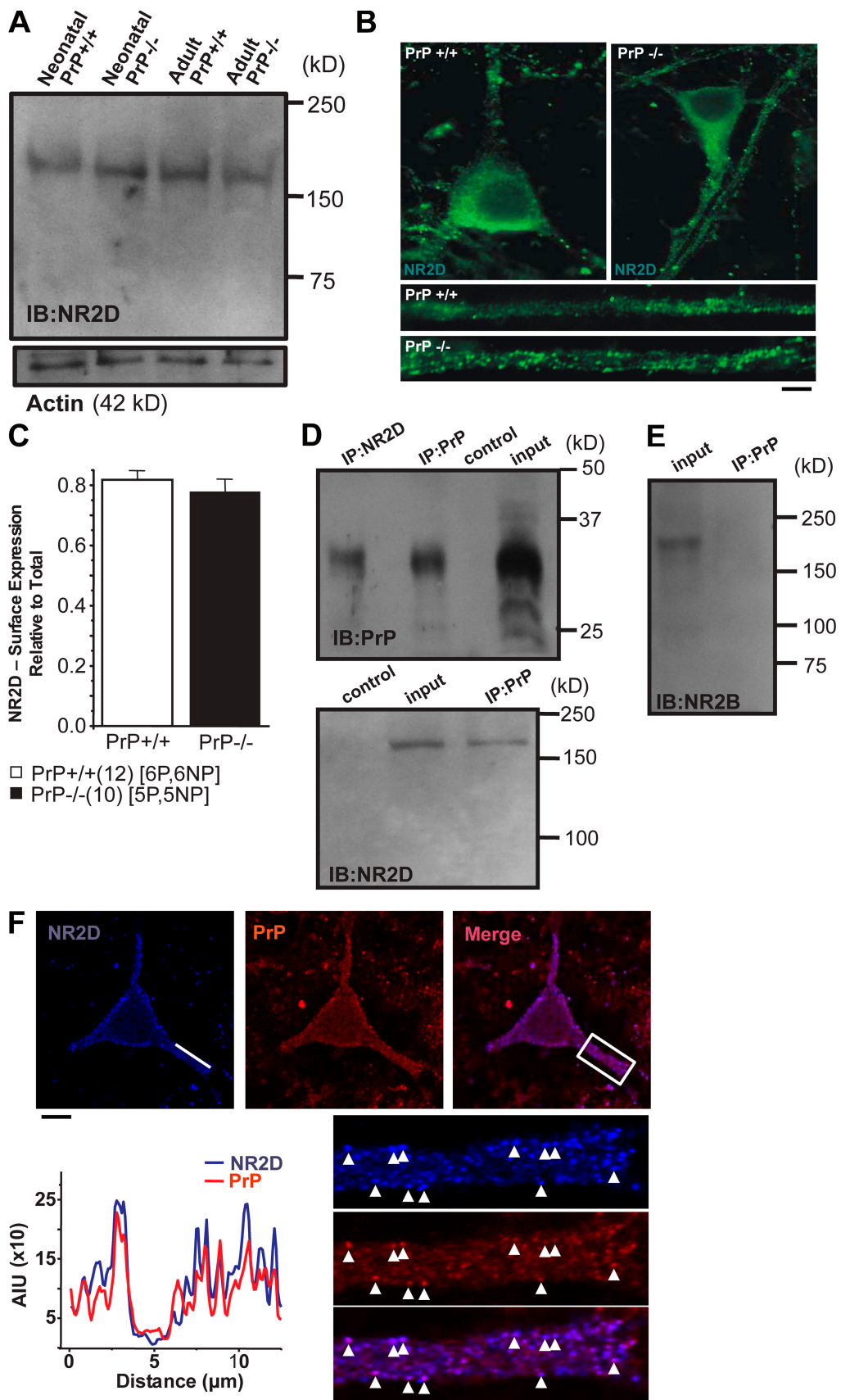


Figure 4. Analysis of the NMDAR NR2D subunit distribution. (A) Western blot analysis of the NR2D subunit protein expression in neonatal and adult hippocampal tissue obtained from the WT and PrP-null mouse. α -Actin expression was used as a loading control. (B) NMDAR subunit surface expression as visualized by immunolabel reactivity with an antibody targeted against an extracellular (N terminus) epitope of NR2D. A punctate pattern of receptor distribution is visualized along dendritic processes. The depth of field is $\sim 1 \mu\text{m}$. (C) Surface expression of NR2D relative to total cellular NR2D protein

exhibited significantly slowed deactivation kinetics compared with those observed in WT neurons irrespective of puff duration (i.e., 50 or 100 ms). This effect was quantified by measuring the time at which current had decayed by 50% (termed time to 50% decay; Fig. 3 B), as the kinetics observed in the PrP-null neurons were too slow to be amenable to exponential fitting. Indeed, some PrP-null neurons yielded NMDA currents that required >10 s to decay, which was never observed in WT neurons. In addition, 50-ms NMDA puffs activated larger currents in the knockout cultures compared with WT cultures, whereas similar current amplitudes were evoked in both cultures when NMDA was puffed for 100 ms (Fig. 3 C). We also applied longer NMDA puffs of 500-ms duration that resulted in a drastic slowing of decay kinetics in both cultures, which was nonetheless still significantly augmented in the null mouse neurons (unpublished data). However, the enhanced slowing at higher NMDA concentrations likely reflects the incomplete clearance of NMDA after the puff rather than pure receptor deactivation. Thus, further analysis was restricted to shorter NMDA puffs. Application of 3 μ M of the NR2B selective inhibitor Ifenprodil resulted in only a $19 \pm 9\%$ ($n = 5$) inhibition of NMDAR current amplitude. In contrast, the same concentration of Ifenprodil mediated a $59 \pm 4\%$ ($n = 8$) inhibition of current amplitude in WT cultures. This observation implies that NR2B-mediated currents comprise a larger proportion of active NMDAR channels in WT neurons. Collectively, these data are consistent with an NMDAR hyperfunction upon knockout of native PrP^C, which is not caused by an augmentation of NR2B-containing receptors. Similar experiments in which GABA_A or AMPA/kainate receptors were activated with agonist puffs did not reveal any differences between WT and PrP-null neurons (Fig. S3, available at <http://www.jcb.org/cgi/content/full/jcb.200711002/DC1>).

To determine whether the slowed NMDA current kinetics in PrP-null mouse neurons were mediated by the long-term absence of PrP^C during in utero development, WT cultures were transfected with three different siRNA constructs directed against the PrP mRNA sequence. PrP expression was observed to significantly decrease in siRNA-transfected neurons (Fig. 3 D). As shown in Fig. 3 E, siRNA knockdown of PrP^C in culture phenocopied the PrP-null mice in that a two-fold increase in NMDAR-mediated current decay time was observed relative to untransfected neurons. Conversely, the overexpression of *Prnp* cDNA in neurons obtained from PrP-null mice rescued the WT phenotype (Fig. 3 F), again hinting at a specific regulation of NMDARs by PrP^C rather than broad developmental effects associated with deletion of the *Prnp* gene. Overall, our data suggest that PrP^C is a negative regulator of NMDAR function in hippocampal neurons.

content as quantified using an ELISA assay in permeabilized (P) and nonpermeabilized (NP) cells. The number of neuronal culture samples is indicated in parentheses. Error bars represent SEM. (D) Coimmunoprecipitation of PrP^C and NR2D using both permutations of tag and probe showing that PrP and NR2D are in a complex. In the top panel, the blot was probed with a PrP antibody, and in the bottom panel, membrane was probed with NR2D antibody. The lane labeled control reflects beads without antibody. The experiment is a representative example of four different repetitions for both neonatal and adult mouse hippocampal tissue. (E) Western blot demonstrating the lack of coimmunoprecipitation between NR2B and PrP^C, whereas NR2B can be detected in brain homogenate (input). (F) Costaining of WT mouse hippocampal neurons for PrP^C (red) and NR2D (blue). The cells were not permeabilized, thus allowing for the selective staining of cell surface protein. The white line in the top left panel indicates the position of the linescan shown in the bottom left panel. The rectangle in the merged image (top right) corresponds to the magnified images shown at the bottom right. The arrowheads highlight examples of clear colocalization between NR2D and PrP^C. Bars: (B, top left) 7.5 μ m; (B, top right and F, top) 10 μ m; (B, bottom) 1 μ m; (F, bottom) 2 μ m.

Expression of NR2D subunits in WT and PrP-null mice

The prolonged current decay kinetics observed in evoked whole cell NMDA currents in PrP-null mice are reminiscent of the slow current waveforms observed upon transient expression of NR1/NR2D receptors in tsA-201 cells (Vicini et al., 1998). This suggests the possibility of a functional upregulation of NR2D-containing receptors in PrP-null mouse neurons. To determine whether the absence of PrP^C triggered the expression of NR2 subunits, NR2D protein expression levels and subcellular distribution were examined in hippocampal neurons of WT and PrP-null mice. As shown in Fig. 4 A, NR2D protein could be detected in hippocampal tissue of both WT and PrP-null mice, irrespective of the age of the animals. Furthermore, RT-PCR analysis indicated that mRNA for all NMDAR subtypes, including NR2D, is present in both WT and PrP-null mouse neurons and at comparable levels (Fig. S4, available at <http://www.jcb.org/cgi/content/full/jcb.200711002/DC1>). The distributions of NR2D receptors in WT and PrP-null mouse neurons were assayed by immunostaining of neurons with an NR2D antibody. As shown in Fig. 4 B, similar distributions of NR2D subunits were observed in both WT and PrP-null mice, with receptors being expressed both on the soma as well as on dendritic processes. Quantitative analysis of the NR2D staining patterns showed no differences in the number of synaptic puncta (PrP^{+/-} and PrP^{-/-}, 46 ± 13 and 43 ± 11 synaptic clusters/100 μ m of dendrite, respectively; $P > 0.9$). Furthermore, the distribution of synapsin I and NR1 subunits, as putative markers of pre- and postsynaptic contacts, was used to rule out the gross synaptic morphological alterations in knockout mice (Fig. S5).

The NR2D antibody used in our study recognizes an extracellular epitope on the NR2D subunit. This allowed us to use luminometry to quantify the fraction of NR2D subunits expressed at the cell surface relative to total NR2D expression by comparing immunoreactivity in permeabilized and nonpermeabilized cells. As shown in Fig. 4 C, in both WT and PrP-null cultures, the NR2D surface expression level amounted to approximately 80% of total NR2D protein. Collectively, these data indicate that hippocampal neurons in both WT and PrP-null mice express similar levels of NR2D surface protein, with no apparent differences in subcellular distributions of NR2D subunits. These data suggest that PrP^C does not act by increasing the amount of NR2D protein at the cell surface. To determine whether NR2D receptor subunits were responsible for the slow current kinetics observed in PrP-null mouse neurons, we transfected knockout neurons with either YFP or YFP plus a set of siRNA constructs directed against NR2D and examined current amplitude evoked by 50- or 100-ms puffs of NMDA.

Elimination of NR2D subunits via siRNA treatment resulted in a drastic reduction in NMDA current amplitude compared with neurons transfected with only YFP ($\text{PrP}^{-/-}$, 299 ± 113 pA, $n = 18$; $\text{PrP}^{-/-}$ with NR2D RNAi, 40 ± 9 pA, $n = 25$; for a 100-ms puff of NMDA). Furthermore, after NR2D knockdown, the kinetics of the remaining NMDA currents were drastically accelerated ($\text{PrP}^{-/-}$, 0.6 ± 0.2 s, $n = 18$; $\text{PrP}^{-/-}$ with NR2D RNAi, 0.21 ± 0.02 s, $n = 25$). Collectively, these data indicate that the slow NMDA currents observed in PrP-null mouse neurons are largely caused by NMDARs containing the NR2D subunit and that these receptors, although present, appear to be functionally silenced by PrP^C .

Given these findings, it is possible that there is a direct regulation of NR2D-containing NMDARs by PrP^C . To examine whether there is a close association of NR2D subunits and PrP^C , we performed coimmunoprecipitations from WT mouse hippocampal homogenate. As shown in Fig. 4 D, PrP^C and NR2D subunits effectively coimmunoprecipitated, indicating that these proteins form a signaling complex. In contrast, NR2B subunits did not immunoprecipitate with PrP^C (Fig. 4 E). Double labeling of WT mouse hippocampal neurons with NR2D and PrP^C antibodies confirmed colocalization between these two proteins (Fig. 4 F). Overall, our data indicate an association of PrP^C with NR2D subunits, which may serve to silence the activities of NR2D-containing NMDARs.

Elevated NMDAR-mediated cell death in $\text{PrP}^{-/-}$ mice

It is well established that NMDARs are important mediators of excitotoxic cell death. In view of the increased NMDAR function in PrP-null mouse neurons, these neurons might show increased susceptibility to glutamate toxicity. To examine this possibility, we transiently (i.e., for 20 min) exposed mature hippocampal cultures to varying concentrations of NMDA, allowed neurons to recover for 24 h, and assayed cell death via TUNEL and trypan blue staining (Fig. 5, A and B). Under control conditions, the percentage of TUNEL-positive cells was similar for WT and PrP-null mouse cultures, whereas a significantly greater percentage of TUNEL-positive cells was observed for PrP-null neurons at a range of different NMDA concentrations (Fig. 5 B). Similarly, transient exposure to NMDA induced a greater percentage of trypan blue-positive neurons in cultures obtained from PrP-null mice (Fig. 5 B). The effect of NMDA on the fraction of TUNEL-positive cells was significantly reduced upon block of NMDARs by the application of APV, thus confirming that NMDA mediated its action via the appropriate receptor.

To determine whether PrP-null mice would exhibit a greater susceptibility to excitotoxic cell death *in vivo*, NMDA was administered by transient focal injection into the hippocampus, and lesion size was quantified by Fluoro-Jade staining. In both WT and PrP-null mice, the lesion size in response to injection of the vehicle was restricted to the damage caused by the insertion of the delivery cannula. Injection of NMDA (10 nmol) resulted in an increase in lesion size that was significantly greater in the PrP-null mice compared with WT animals (Fig. 6, A and B). This observation is in agreement with our findings in cultured hippocampal neurons. Collectively, these data show that

PrP-null mice exhibit an enhanced susceptibility to NMDAR-mediated excitotoxicity, which is consistent with the enhanced NMDAR activity observed in these animals.

Discussion

Since its discovery as an endogenous protein, the physiological functions of PrP have remained incompletely defined. The particularly high level of expression of PrP^C in nervous tissue has pointed to a functional role in neuronal and/or glial elements. PrP^C has been localized to synaptic contacts, suggesting a possible role in synaptic physiology. However, its precise localization within pre- and/or postsynaptic membranes requires further investigation (Herms et al., 1999; Fournier et al., 2000). A possible role of PrP^C in synaptic function is supported by the notion that PrP-null mice display impaired spatial learning and altered excitatory and inhibitory neurotransmission (Collinge et al., 1994; Criado et al., 2005). Our findings showing that deletion of the PrP gene in mice results in altered synaptic NMDAR function is consistent with an important role of PrP in synaptic function.

The synaptic properties of PrP-null mouse neurons have been subject to previous investigation by other laboratories. Collinge et al. (1994) reported the presence of additional population spikes in extracellular CA1 field recordings of PrP-null mice, which agrees with our observations. However, Collinge et al. (1994) attributed this effect partly to impaired GABAergic signaling as reflected in reduced IPSP amplitudes and increased rise and decay times. Although the rise and decay times of GABAergic mIPSCs were slightly increased in null mouse cultures, we did not observe any changes in agonist-evoked GABA_A currents, and IPSC amplitude was unaffected in our hands. Instead, the enhanced number of population spikes was greatly reduced or abolished upon application of the NMDAR antagonist APV, indicating that the increase in excitability was mainly caused by an NMDAR-mediated action. In contrast, Lledo et al. (1996) failed to observe any alterations of either excitatory or inhibitory synaptic transmission. Similarly, Carleton et al. (2001) failed to observe multiple population spikes in the PrP-null mice. However, in both of these studies, slice experiments were conducted at room temperature rather than at 32°C, a condition under which we noted a similar loss of excitability of the null mouse cultures. In recordings conducted at 28°C, Maglio et al. (2004, 2006) did not report gross alterations in the shape of field potentials; however, no quantification of numbers of population spikes was conducted. In Purkinje neurons, no difference between WT and PrP-null mice was reported for GABAergic and glutamatergic synaptic currents (Herms et al., 1995). These authors conducted their recordings in the presence of extracellular Mg^{2+} , which eliminates NMDAR-mediated synaptic currents and thus isolates the AMPA receptor-mediated component. Thus, their data showing normal synaptic AMPA currents are in agreement with our findings. Our observation that paired-pulse facilitation, as assessed in the CA1 layer of the hippocampus, was not different between WT and PrP-null mice is consistent with previous studies (Carleton et al., 2001; Curtis et al., 2003). Finally, we note that Criado et al. (2005) recorded field responses from hippocampal neurons in

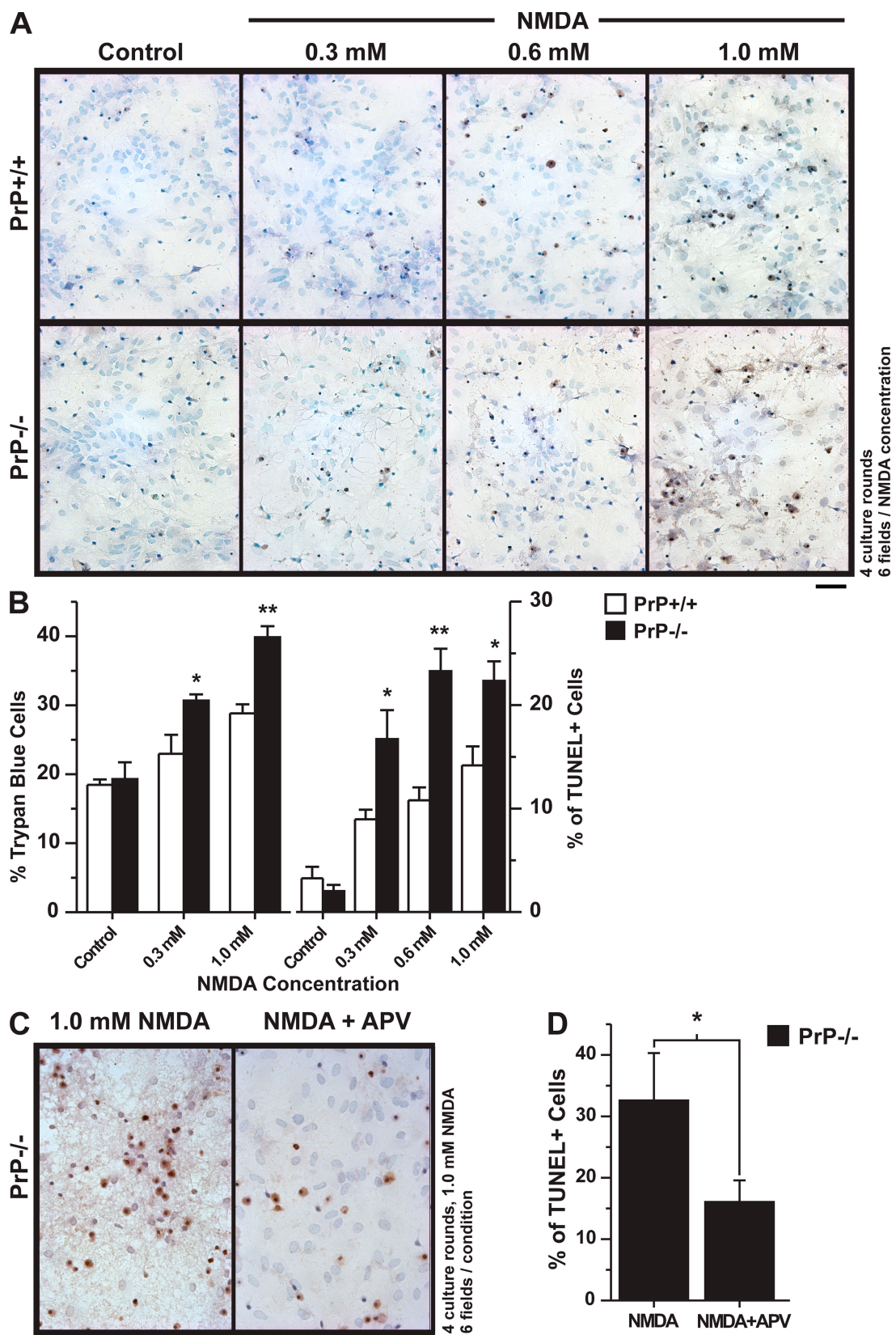
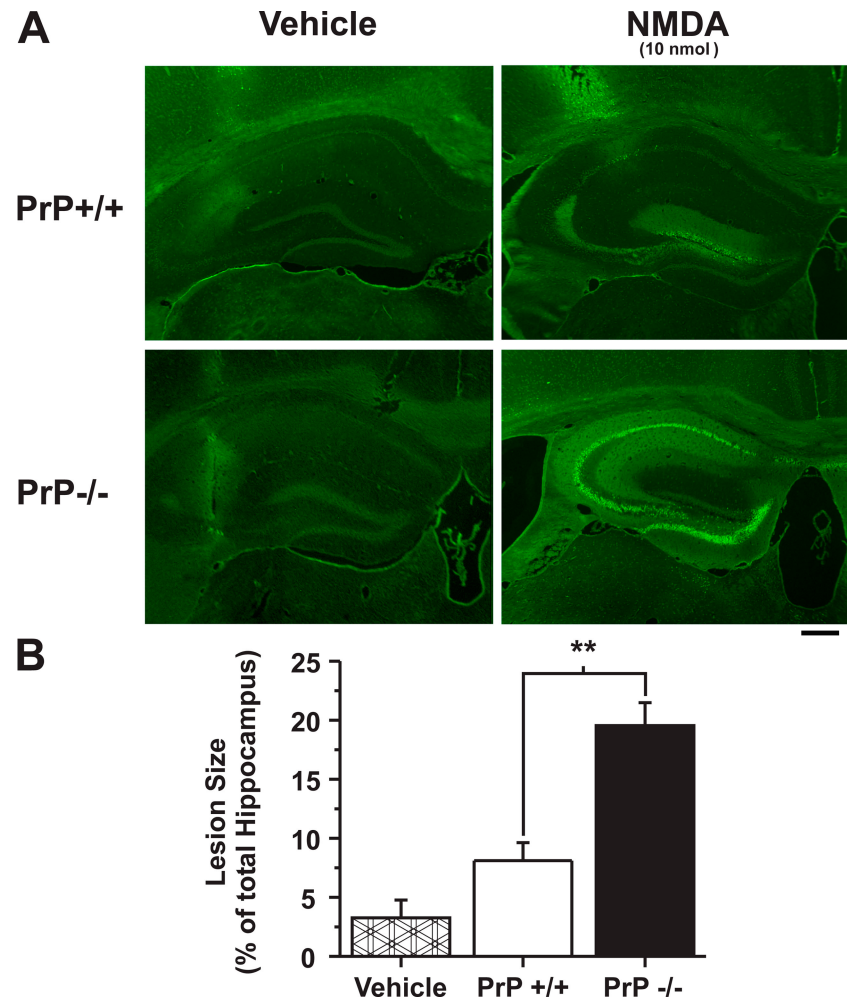


Figure 5. NMDAR-mediated excitotoxic cell death in PrP-null neurons. (A) Light microscope images of neuronal cultures after 20 min of exposure to 0.3, 0.6, and 1.0 mM NMDA followed by 24-h recovery. Cells were stained with trypan blue (dark blue) and TUNEL (brown); methyl green was used as the counter-stain. (B) Mean cell counts for trypan blue- and TUNEL-stained cells in WT and PrP-null cultures. (C) Light microscope images showing TUNEL-stained neurons from PrP-null mice in the presence of NMDA and NMDA + APV. (D) Percentage of TUNEL-positive neurons from PrP-null mice in response to NMDA and NMDA + APV. The drug concentrations were 1 mM NMDA and 100 μ M APV. Data are represented as mean \pm SEM (error bars), with statistical significance denoted as *, P < 0.05 and **, P < 0.001. Data were obtained from four culture rounds, and six random fields were imaged per condition. Bar, 100 μ m.

Figure 6. Increased excitotoxic cell death and lesion size in the hippocampus of PrP-null mice in response to in vivo transient NMDA exposure. (A) Fluoro-Jade labeling of neuronal bodies and processes in hippocampal sections in response to injection of vehicle (left) or NMDA (10-nmol equivalent; right). (B) Quantification of lesion size relative to the hippocampus over a series of three to six sections per animal ($n = 5$ per experimental group). Data are represented as mean \pm SEM (error bars), with statistical significance denoted as **, $P < 0.001$. Bar, 200 μ m.



vivo and found that stimulus threshold and population spike height were similar in WT and knockout animals. However, these experiments were conducted on the *Edinburgh* PrP knockout mouse strain rather than the *Zurich* mice used in our study, thus precluding firm comparisons. Indeed, there are several knockout mouse lines that lack *PrP^C* (Sakudo et al., 2006; Steele et al., 2007), and these may account for some of the observed differences.

Our data show a robust enhancement of synaptic NMDA currents in PrP-null mice, which could be mimicked upon siRNA depletion of PrP^C and rescued by overexpression of exogenous *Prnp* cDNA. The enhancement and broadening of NMDAR-mediated mEPSCs could, in principle, be the result of either pre- or postsynaptic effects such as increased quantal content, impaired glutamate reuptake, or enhancement of NMDAR function in the postsynaptic membrane. The unaltered degree of paired-pulse facilitation fits with a postsynaptic mechanism of action. The broadening and increased amplitude of the mEPSCs is consistent with our evoked whole cell recordings showing an apparent enhancement of NMDA affinity and prolonged current deactivation kinetics in response to direct activation of the receptors. Thus, although we cannot rule out the possibility of a contribution from presynaptic effects, our data are most consistent with a post-synaptic action of PrP^C by virtue of altered NMDAR function.

Previous *in situ* hybridization experiments have suggested that NR2A and NR2B but not NR1 mRNA may be upregulated in both young and adult PrP-null mice (Maglio et al., 2004, 2006), which is not supported by our semiquantitative PCR experiments. Furthermore, several lines of evidence suggest that the enhanced NMDA currents in cultured neurons are not caused by an enhanced expression of NR2A and/or NR2B subunits. NR2A subunit-containing receptors (which comprise the bulk of the synaptic NMDARs in adult neurons) typically exhibit the most rapid decay kinetics among all NMDAR isoforms, whereas NR2B receptors deactivate more slowly (Cull-Candy and Leszkiewicz, 2004). The observation that the NR2B antagonist Ifenprodil did not block the slow NMDA currents in PrP-null mouse neurons suggests that the observed kinetic slowing is not caused by a switch from NR2A- to NR2B-containing receptors upon deletion of the PrP gene. Moreover, the current decay kinetics observed in the PrP-null neurons were much slower than those expected for NR2B-containing receptors and instead resembled those observed with transiently expressed receptors containing NR2D subunits (Vicini et al., 1998). Consistent with such a mechanism, siRNA depletion of NR2D subunits greatly diminished (and accelerated) the NMDA currents seen in PrP-null mouse cultures. WT and PrP-null mouse neurons both expressed NR2D subunit mRNA and protein, with ~80%

of NR2D protein expressed at the cell surface. Because isolated NR2 subunits do not traffic to the plasma membrane unless they are in a complex with an NR1 subunit (Dunah et al., 1998; Cull-Candy and Leszkiewicz, 2004), the NR2D receptors expressed in the plasma membrane of WT mouse neurons are likely part of fully assembled NMDAR complexes. This implies that the NR2D-containing NMDARs in WT neurons are electrically silent. Thus, the presence of PrP^C in these neurons appears to impair NR2D receptor function rather than primarily regulating receptor trafficking. It is important to note that NR2D-like synaptic miniature currents have, to our knowledge, never been demonstrated in WT hippocampal neurons, which is consistent with tonic inhibition of these receptors by PrP^C.

PrP^C and NR2D subunits could be coimmunoprecipitated from hippocampal homogenate, indicating that NR2D-containing receptors form a protein complex with PrP^C, but it is unclear exactly how PrP^C functionally inhibits NMDAR activity. The fact that functional NR1/NR2D currents can be recorded in tsA-201 cells even though these cells express endogenous PrP^C might argue against a direct silencing of NR2D-containing receptors. However, exogenously expressed NMDAR subunits may outnumber endogenous PrP^C levels in these cells, thus leaving the possibility of a direct regulation of NR2D-containing receptors by PrP^C. This could occur by mechanisms such as a PrP^C-mediated stabilization of closed states or interference with glutamate or coagonist binding. Alternatively, NMDARs are known to be potently regulated by several protein kinases and phosphatases (Wang and Salter, 1994; Dalva et al., 2007), and it is thus possible that PrP^C activates second messenger pathways that inhibit the function of NR2D-containing receptors. Future experimentation will be required to dissect the mechanisms by which PrP regulates NMDAR activity. However, irrespective of the molecular mechanisms underlying the observed effects, our data support a major role of PrP^C in regulating NMDAR function.

The notion of enhanced NMDAR activity in PrP-null mouse neurons is consistent with the enhanced NMDA toxicity observed in our *in vitro* and *in vivo* studies and indicates that PrP^C provides a degree of neuroprotection from glutamate toxicity. This is supported by the recent findings of Rangel et al. (2007), who reported that kainic acid application mediates increased cell death in organotypic brain slices cultured from PrP-null mice. Intriguingly, this effect was attenuated by the NMDAR inhibitor MK-801, suggesting that activation of kainate receptors in this model may cause its toxic effects indirectly via NMDARs, perhaps by depolarization-induced Mg²⁺ unblock. Our findings showing increased NMDAR activity in null mice would be consistent with such a mechanism. Similarly, the enhanced cell death observed in pharmacologically induced seizure models seen with PrP-null mice may be related to NMDAR hyperfunction. The role of glutamate-dependent neuronal death involving NMDARs is also a key feature of ischemic stroke (Arundine and Tymianski, 2004). In this context, it is interesting to note that a recent study has demonstrated an upregulation of endogenous PrP in response to acute ischemic stroke in rats and also reported elevated PrP plasma levels in human stroke patients (Mitsios et al., 2007). Furthermore, increased levels

of PrP are detectable in surviving neurons localized to the peri-infarct region (Weise et al., 2004; Mitsios et al., 2007). This raises the intriguing possibility that enhanced PrP expression may be a compensatory mechanism to protect from NMDAR-mediated cell damage during ischemic insults.

It is unclear how NMDAR-mediated cell death contributes to the etiology of prion disease. During the development of prion disease, endogenous PrP^C is progressively misfolded, resulting in the formation of PrP^{Sc} aggregates and, as has recently been shown, in a significant knockdown of endogenous PrP^C levels (Griffin et al., 2007). This type of depletion of normal PrP^C levels may well mimic some aspects of the phenotype of PrP knockout (such as enhanced NMDAR activity). This alone cannot account for the disease progression because PrP-null mice are intrinsically resistant to the infectious form of PrP, and deletion of the *Prnp* gene rescues animals from disease progression (Mallucci et al., 2007). Furthermore, although PrP-null mice were recently shown to exhibit some evidence of spontaneous neurodegeneration with age (Nazor et al., 2007), they do not develop classical and fatal TSE, indicating that normal endogenous glutamate levels are insufficient to trigger massive NMDAR-mediated toxicity in the absence of PrP. However, it is likely that the accumulation of PrP^{Sc} aggregates on neurons and glial cells (Rezaie and Lantos, 2001) results in enhanced glutamate levels in the diseased brain as caused by cell damage. In conjunction with enhanced NMDAR function caused by lower normal PrP^C levels, this could ultimately contribute to the excitotoxic cell death of neurons observed in TSEs. Indeed, this would fit with previous studies showing that scrapie-infected neuronal cultures and cultures treated with infectious prion fragments show increased neuronal survival upon NMDAR blockade (Muller et al., 1993; Brown et al., 1997; Sassoon et al., 2004). However, such putative linkages need to be further explored experimentally.

In summary, our results identify PrP^C as a regulator of NMDAR function and demonstrate that PrP^C exerts a neuroprotective role by inhibiting aspects of NMDAR activity linked to excitotoxic cell death. The regulation of synaptic NMDARs implicates PrP^C as a modulator of synaptic function and, consequently, neuronal excitability.

Materials and methods

PrP-null mice

Mice with a targeted disruption of the prion gene (*Prnp*) of the Zürich 1 strain (Bueler et al., 1992) and their controls (both of a mixed 129 and FVB background) were obtained from the European Mouse Mutant Archive (EM:0158; European Mouse Mutant Archive Rome) and interbred to generate PrP^{-/-} (PrP null) and PrP^{+/+} (WT) littermates used in the experiments. Genotyping was performed by gel electrophoresis of PCR products obtained from genomic DNA that was isolated from tail samples. Primers and PCR parameters were similar to those used previously (Bueler et al., 1992). Comparisons were made between electrophysiological recordings obtained from offspring pups (WT and PrP^{-/-} littermates) from the original breeding pairs or from offspring obtained from PrP^{+/+} × PrP^{+/+} or PrP^{-/-} × PrP^{-/-} crosses; in all instances, the results were indistinguishable ($n > 20$ in each case), indicating that the variability in genetic background had no detectable effect on the observed phenotype. The experimentalists were blinded to the genotype of the mice for greater than half of the electrophysiological experiments ($n > 30$ for each genotype) and became unblinded when no differences were identified that suggested an experimenter-dependent segregation of results.

Brain slices

Adult male and female WT mice between P30 and P45 were used for all slice experiments. Mice were anaesthetized with halothane and quickly decapitated. The brain was dissected and maintained in ice-cold aCSF for ~1 min. 250- μ m horizontal hippocampal slices were obtained at an angle of 12° in the frontal-occipital direction (Vibratome 1000; Vibratome, Inc.) while submerged in ice-cool oxygenated aCSF. The slices were immediately transferred to a holding chamber, where cool oxygenated aCSF was gradually warmed to 32°C at the end of the sectioning and maintained at that temperature for 2–5 h for subsequent electrophysiological recordings. All slices were allowed a minimum of 1 h of recovery before experimentation. Tissue samples used for all biochemical and/or protein biochemistry experiments consisted of the isolated whole intact hippocampus (from each hemisphere) as quickly dissected on an ice-cold surface with regular perfusion of cold oxygenated aCSF.

Neuronal primary culture and transfection

Dissociated hippocampal neurons were prepared as previously described (Khosravani et al., 2005). Electroporation was used to introduce exogenous plasmid (either cDNA or siRNA) constructs into the cells; this was performed after trituration, while cells were in suspension and before plating. 3–5 μ g of enhanced YFP was used as the transfection marker. The electroporation protocol consisted of the following: voltage of 100 V, square pulse duration of 100 ms, one pulse, and a 4-mm cuvette (X-Cell; Bio-Rad Laboratories). All data obtained from neuronal culture-based experiments were obtained from at least three separate culture rounds.

Molecular biology

Mouse *Prnp* cDNA (GenBank/EMBL/DDBJ accession no. BC006703) was cloned into pCMV-SPORT6 (Open Biosystems); this construct was used for PrP reconstitution experiments. For siRNA experiments, we used mouse retroviral short hairpin RNA (shRNAmir) with individual clones spanning different regions of the *mPrnp* sequence (clone ID RMM1766-98468689, RMM1766-96744825, and RMM1766-9336256) cloned in pSHAG-MAGIC2 (Open Biosystems). All three siRNA constructs were cotransfected into neurons. For NR2D RNAi experiments, we used the following shRNAmir constructs: clone ID TRCN0000100210, TRCN0000100211, TRCN0000100212, TRCN0000100213, and TRCN0000100214. Each construct was tested independently in transfection experiments to evaluate knockdown efficiency, and the 212 and 214 constructs were used for knockdown and produced identical results, which were pooled. To achieve maximum purity, plasmids were prepared using the endonuclease-free Maxiprep kit according to the manufacturer's instructions (QIAGEN).

RT-PCR analysis of NMDAR subunit and PrP expression

Total mRNA was isolated from adult (P30–45) or neonatal (P0–1) hippocampal homogenate using TRIzol. The quality of RNA was analyzed by agarose gel electrophoresis and ethidium bromide staining by standard methods. The mRNA was reverse transcribed using Superscript III and oligo-dT primers. Approximately 5 μ g of total RNA was used for each reverse transcription reaction. Afterward, the first-strand synthesis RNA was digested by treatment with RNase H. The single-stranded cDNA was stored at –20°C until it was used for PCR amplification. These experiments were performed in a blinded manner and performed on tissues obtained from two or more independent pairs of WT and PrP-null animals. Synthetic oligodeoxynucleotides based on the four known mouse NR2 subunit sequences and mouse PrP were synthesized (University of Calgary DNA synthesis facility). For each receptor subtype, two different regions of mRNA sequence were selected: a region in the 5' half and another close to the 3' end region. Additionally, one primer set was designed for amplification of γ -actin. Primer sequences are shown in Table S1 (available at <http://www.jcb.org/cgi/content/full/jcb.200711002/DC1>), and representative experimental results are shown in Fig. S4.

Electrophysiology

All slice and cultured cell recordings utilized a standard extracellular solution (aCSF) containing the following: 125 mM NaCl, 5 mM KCl, 1.25 mM NaH₂PO₄, 2 mM MgSO₄, 1.5 mM CaCl₂, 25 mM NaHCO₃, and 10 mM D-glucose, pH 7.4, when bubbled with 95% O₂ and 5% CO₂. The osmolarity was 310 ± 5 mosM. For recording seizure-like events, in a model of spontaneous recurrent seizures, the superfusing aCSF was switched to one that lacked MgSO₄. All field recordings were performed in the CA1 layer of the hippocampus. Evoked (orthodromic) field responses were delivered using a bipolar stimulating electrode placed in the Schaffer collaterals. The stimulus was generated by a constant voltage stimulator (DS2A-MKII; DigiTimer)

with pulse delivery under computer control. The minimum stimulus intensity was obtained by noting the stimulus intensity required to evoke the first instance of a population spike using the first pulse. Maximum stimulus threshold was determined at the stimulus intensity at which the amplitude of the population spike reached a plateau. Stimulus intensity was fixed at 80% of maximum for other experiments, including zero-magnesium and pharmacology experiments involving APV. Extracellular potentials were recorded using a patch pipette filled with 150 mM NaCl.

Successful whole cell voltage and current clamp recordings were obtained from neuronal cultures between DIV 10 and 16. Miniature postsynaptic currents were recorded in voltage-clamp mode from putative pyramidal neurons using either Axopatch 200B or Multiclick 700B amplifiers (MDS Analytical Technologies). For recording excitatory (i.e., AMPA/kainate and NMDA) mEPSCs, a holding potential of –60 mV was used to obtain maximal responses. Inhibitory GABA_A mIPSCs were recorded at a holding potential of 10 mV. Current clamp recordings were made in I-Fast mode with cells hyperpolarized to –70 mV. The intracellular solution for voltage-clamp experiments contained the following: 100 mM Cs-gluconate, 1.7 mM CsCl, 10 mM EGTA, 5 mM MgCl₂, and 40 mM Hepes adjusted to pH 7.3 with CsOH. The intracellular solution for current clamp experiments contained the following: 100 mM K-gluconate, 1.7 mM KCl, 0.6 mM EGTA, 5 mM MgCl₂, and 40 mM Hepes adjusted to pH 7.25 with KOH. Both internal solutions were supplemented with 2 mM Tris-ATP, 0.5 mM Na-GTP, and 5 mM phosphocreatine.

The standard extracellular bath solution was aCSF. The following agonists and antagonists were used for isolating specific synaptic currents: for recording AMPA/kainate EPSCs, we used 0.5 μ M TTX (Alomone) and 100 μ M picrotoxin (Sigma-Aldrich) in standard 2 mM Mg²⁺. For isolating NMDA EPSCs or whole cell currents, we used 15 μ M CNQX (6-cyano-7-nitroquinoxaline-2,3-dione disodium salt) and 20 μ M glycine, which were added to a zero-magnesium aCSF in the presence of TTX and picrotoxin. For NMDA puff experiments requiring selective block of NR2B-containing receptors, we included 3 μ M Ifenprodil in the extracellular and pipette solutions. Miniature GABAergic IPSCs were recorded in aCSF with 2 mM Mg²⁺ in the presence of CNQX and TTX. Current clamp recordings were performed in the absence of any drugs. All experiments were performed at 32 ± 1°C with perfusion rates near 1–2 ml/min. Patch electrodes had tip resistances ranging from 5 to 8 M Ω when filled with internal solution; series resistance was compensated by 80%. For current clamp recordings, only neurons with input resistances <250 M Ω and resting membrane potentials more hyperpolarized than –50 mV were considered for analysis. Electrophysiological data were acquired in pClamp 9.2 using a DigiData 1322A (MDS Analytical Technologies). For voltage-clamp recording, data were filtered at 2 kHz with an eight-pole low-pass filter and sampled at 10 kHz; current clamp recordings were filtered at 10 kHz and sampled at 50 kHz. Recordings of spontaneous excitatory miniatures were analyzed using MiniAnalysis (Synaptosoft, Inc.). All other recordings were processed using an in-house software package developed in Matlab (Mathworks). Mean values for miniature postsynaptic current parameters were calculated as a mean of means. Specifically, a mean value (e.g., mEPSC amplitude) was computed for all events recorded in a cell and averaged for subsequent comparison between WT and PrP-null animals. Raw values were used for calculating cumulative probability. In instances in which the total number of events was different between WT and PrP-null conditions (e.g., 450 mEPSCs in WT and 700 in knockout), we used SPSS software to randomly sample 450 events from the 700, and these were used for subsequent analysis. This was done in order not to bias the calculation of cumulative ensemble-type statistics. Cumulative probability plots were compared, and significant differences were established for P < 0.05 using the Kolmogorov-Smirnov test.

For NMDA puff experiments, a second micromanipulator with a patch pipette was brought in the vicinity of the cell soma; position and distance were kept as constant as possible using video guidance with designated markings on the viewing monitor for cell center in relation to the puff electrode placement. NMDA was applied at a concentration of 100 μ M (made in external solution) and a pressure of 8 psi; the electrode tip diameters were similar to those used for the whole cell patch experiments. The three puff durations used (50, 100, and 500 ms) were computer controlled for timing and initiation using a DigiData 1322A interface (MDS Analytical Technologies) to deliver the transistor-transistor logic pulse. Analogous protocols were used for GABA and AMPA puff experiments.

Immunofluorescence microscopy of neuronal cultures

Cells were grown on glass coverslips, briefly rinsed with PBS, and fixed for 15 min with 4% PFA at room temperature. Coverslips were rinsed three

times with PBS and after blocking nonspecific binding with blocking buffer (3% BSA in PBS). They were incubated overnight at 4°C with the primary antibody in blocking buffer. Pre- and postsynaptic contacts were visualized by costaining with anti-synapsin-I (1:1,000; Chemicon) conjugated with AlexaFluor568 goat anti-rabbit IgG (1:1,000; Invitrogen) and anti-NR1 (1:500; Synaptic Systems GmbH) conjugated with AlexaFluor488 goat anti-mouse IgG (1:1,000; Invitrogen). NR2D subunit distribution was detected using a polyclonal antibody raised against a peptide mapping to the N terminus of the NR2D subunit, anti-NR2D (R-20; 1:200; Santa Cruz Biotechnology, Inc.), conjugated with either AlexaFluor488 or 568 donkey anti-goat IgG. For NR2D and PrP colocalization, NR2D (1:200; Santa Cruz Biotechnology, Inc.) and mouse monoclonal anti-PrP (1:200; Chemicon) antibodies were used and conjugated to AlexaFluor488 IgG and AlexaFluor546 IgG, respectively. Secondary antibodies were used at a 1:1,000 dilution. After secondary staining, the coverslips were subjected to three washing cycles with PBS and were stored in PBS containing a drop of Vectashield antifade reagent (Vector Laboratories). All immunostaining of neuronal cultures was repeated on a minimum of two independent culture rounds for NR1 and greater than three for NR2D and PrP.

All epifluorescence imaging was performed on an upright microscope (Axioskop 2 FS; Carl Zeiss, Inc.) with infrared differential interference contrast and fluorescence capability. Images were visualized through water immersion objectives (either Achromplan 40× 0.8 NA or Achromplan 63× 0.95 NA; Carl Zeiss, Inc.). Epifluorescence was visualized through dichroic mirrors with the following excitation/emission filter properties: 450–490/515–565 nm (green channel), 500–520/535–565 nm (yellow channel), and 530–585/long-pass 615 nm (red channel). Imaging was typically performed using unmounted coverslips in PBS. Images were acquired using a CCD camera with on-chip signal integration (120N; Watec) and sampled by a high resolution video capture card. Confocal imaging was performed using a microscope (LSM510 Meta; Carl Zeiss, Inc.) with a 63× 1.4 NA oil immersion objective (Carl Zeiss, Inc.). The entire cell volume was imaged by a series of z-plane sections, resulting in z-stacks. Fluorescence was visualized via laser excitation and emission, with sequential activation detected using dichroic and filter optics with the following excitation/emission properties: 488/long pass 505 nm (for NR2D) and 543/long pass 585 nm.

Coimmunoprecipitations and immunoblotting

The hippocampal region was quickly dissected under a microscope (SMZ645-660; Nikon) and used as a sample. Neonatal samples were collected from P0–1 pups, whereas adult samples were obtained from P30–45 mice. The tissue was homogenized by a Dounce homogenizer in cold lysis buffer (300 mM NaCl, 10 mM Tris-Cl, pH 8.0, and 0.5% Triton X-100 plus protease inhibitor cocktail [Roche]). After incubating on ice for 1 h, the supernatant was collected. The homogenate was centrifuged at 10,000 g for 20 min at 4°C, supernatant was collected, and the protein concentration was determined using the Protein Assay kit (Bio-Rad Laboratories). Subsequently, 20–30 µg of protein was loaded per lane onto a 10% SDS polyacrylamide gel, and Western blot analysis was performed. The following antibodies were used for the blots: anti-NR2D at 1:200 (Santa Cruz Biotechnology, Inc.), anti-NR2B at 1:500 (Calbiochem), and anti-PrP at 1:200 (Santa Cruz Biotechnology, Inc.). After 2 h at room temperature, the membrane was washed three times in the PBS containing 0.5% Tween 200 for 30 min and incubated for 1 h in HRP-conjugated second antibody (1:10,000). Antigen was detected using enhanced chemiluminescent HRP substrate (ECL; GE Healthcare). Immunoreactive bands were visualized after exposure of the membranes to Hyperfilm MP (GE Healthcare).

For immunoprecipitation, 70 mg of tissue was homogenized by Dounce homogenizer in 500 µl of cold lysis buffer with protease inhibitor. The sample was left on ice for 1 h and spun at 10,000 g for 20 min at 4°C, and supernatant was collected. 100 µl of lysate was diluted to 500 µl with lysis buffer (5 mM Tris, pH 7.5, 300 mM NaCl, 0.5% Triton X-100, and a cocktail of protease inhibitor) and precleared by 25 µl of protein A/G Sepharose (GE Healthcare) for 30 min. The solution was spun at high speed, and supernatant was collected. 5 µg of antibody was then added to lysate and incubated at 4°C overnight. 50 µl of protein A/G Sepharose was then added to collect the immunoprecipitate. Samples were incubated 4°C for 2 h and centrifuged at 800 rpm for 1 min, and supernatant was collected. The precipitate was washed three times with 1 ml of lysis buffer. 50 µl of 2× sample buffer was added to each sample and run on an SDS polyacrylamide gel. 20 µl of each sample was loaded onto the gel. Separated protein were transferred to nitrocellulose and probed with various antibodies. These experiments were performed in a blinded manner and using tissues obtained from a minimum of three independent pairs of WT and PrP-null animals.

ELISA assays

Hippocampal neurons (DIV 14) were fixed in 4% PFA followed by two 5-min washes with PBS. Half of the cells were permeabilized with 0.1% Triton X-100 for 5 min followed by a 30-min incubation in blocking solution (PBS + 3% BSA). The expression of NR2D was measured using an antibody raised against a peptide mapping to the N terminus of the NR2D subunit (R-20; 1:200; Santa Cruz Biotechnology, Inc.) and an HRP-conjugated donkey anti-goat (1:1,000; Jackson ImmunoResearch Laboratories). SuperSignal ELISA femto maximum sensitivity substrate (Thermo Fisher Scientific) was added, and luminescence was measured with a luminometer (Victor 2; PerkinElmer) as described previously (Altier et al., 2006). The ratio between signals obtained from nonpermeabilized (i.e., surface expression) and permeabilized neurons (i.e., total expression) was then calculated from 12 coverslips (six permeabilized and six nonpermeabilized) with WT and 10 coverslips with PrP-null neurons.

In vitro excitotoxicity assays

Primary hippocampal cultures between DIV 16 and 18 were used in NMDA excitotoxicity assays. Coverslips were transferred to a new 24-well dish with fresh medium. Cells were exposed to vehicle (control) or NMDA at varying concentrations (0.3, 0.6, and 1.0 mM) for 20 min. Coverslips were then transferred back to their originating wells and allowed to recover for 24 h after exposure. Cells were exposed to trypan blue dye (0.4% stock diluted to 1:100) for 1 min. Coverslips were washed in 3× PBS and fixed with 4% PFA. These coverslips were then stained with a TUNEL cell death detection kit (Chemicon), and the number of TUNEL-positive cells was counted for each NMDA concentration. Imaging was performed in PBS for trypan blue-stained cells and on mounted coverslips for TUNEL-stained cells. For each imaging session, six randomly selected fields were imaged using conventional light microscopy (40×). Within each field, the total number of cells was visualized by either differential interference contrast (for trypan blue) or via counterstaining with methyl green (for TUNEL). The number of trypan blue and TUNEL cells were counted during independent imaging sessions. The number of positively stained cells (either trypan or TUNEL) was reported as a fraction of the total number of cells taken as a mean over the imaged fields. All in vitro excitotoxicity experiments were repeated using at least two independent culture rounds.

Lesion surgery and Fluoro-Jade staining

10–12-wk-old mice were anesthetized with ketamine/xylazine given at a dose of 85/15 mg/kg intraperitoneally and were mounted in a stereotaxic frame (Kopf Instruments). The mice received hippocampal injections of 1 µl of a solution containing 10 nmol NMDA in PBS with the following stereotaxic coordinates: 2.0 mm caudal to bregma, 2.0 mm lateral to midline, and 2.0 mm ventral from the bone surface. NMDA was injected over 5 min, and the needle was left in place for an additional 5 min to minimize the leakage. Animals were maintained according to Canadian Council on Animal Care guidelines, and this study was approved by the University of Calgary Animal Care Committee. 48 h after NMDA injection, mice were deeply anesthetized with ketamine/xylazine and transcardially perfused with PBS followed by 4% PFA in PBS. The brains were removed, placed in 4% PFA overnight at 4°C, and dehydrated in 20% sucrose/PBS for 1 d. The brain samples were frozen in optimal cutting temperature compound (Sakura Finetek) at –80 °C. 25-µm coronal sections were cut by cryostat, mounted on the slide glass, dried, and immersed in 100% ethanol followed by 70% ethanol. Sections were then treated with 0.06% potassium permanganate for 15 min, rinsed by PBS, and immersed in Fluoro-Jade C (0.001% in 0.1% acetic acid; Histo-Chem, Inc.) for 30 min. After rinsing, sections were dried and mounted with xylene-based mounting media for analysis.

Statistics

Statistical analyses were performed using SigmaStat (SPSS, Inc.). Unless stated otherwise, statistical significance was evaluated using *t* tests for comparing two groups and one-way analysis of variance for comparison of multiple groups versus control using the Bonferroni posthoc test. Statistical significance was reported for quantities with $P < 0.05$ (single asterisk) and $P < 0.001$ (double asterisks).

Spectral analysis of epileptiform discharges

Fourier-based analysis was used to characterize the cumulative power spectral amplitude for each discharge (Fig. S1). This was computed for five frequency bands (0–500 Hz; 100-Hz increments for each bandwidth). The analysis was performed for 500 randomly selected discharges each from seizure-like events in WT ($n = 18$) and PrP-null ($n = 21$) slices. All calculations were conducted using Matlab software.

Online supplemental data

Fig S1 shows power spectral analysis of frequencies within seizure-like discharges recorded in ZM-aCSF for WT and PrP-null slices. Fig S2 shows alterations in spontaneous AMPA and GABA_A receptor-mediated synaptic transmission. Fig S3 shows kinetic analysis of AMPA/kainate and GABA_A receptor-mediated currents in cultured hippocampal neurons from WT and PrP-null mice. Fig S4 shows RT-PCR analysis of NMDAR subtypes present in the isolated hippocampi of neonatal and adult mice for both WT and PrP-null genotypes. Fig S5 shows synapsin I (presynaptic protein) and NR1 (postsynaptic protein) expression patterns as visualized in WT and PrP-null mature primary hippocampal cultured neurons. Table S1 shows primer sequences for RT-PCR analysis. Online supplemental material is available at <http://www.jcb.org/cgi/content/full/jcb.200711002/DC1>.

We thank Drs. Jaideep Bains, Ray Turner, Bin Hu, and Robert Messing for helpful comments on this work. We would like to thank Ms. Latha Narayanan for initially maintaining the PrP animal lines.

H. Khosravani holds MD/PhD scholarships from the Alberta Heritage Foundation for Medical Research (AHFMR) and the Canadian Institutes of Health Research (CIHR). S. Tsutsui holds a fellowship from the Multiple Sclerosis Society of Canada. F.R. Jirik holds a Canada Research Chair in Molecular Medicine. G.W. Zamponi holds a Canada Research Chair in Molecular Neurobiology and is an AHFMR Scientist. This study was supported by grants from the Canadian Genetic Diseases Network, the Alberta Agricultural Research Institute, and the CIHR.

Submitted: 1 November 2007

Accepted: 28 March 2008

References

- Altier, C., H. Khosravani, R.M. Evans, S. Hameed, J.B. Peloquin, B.A. Vartian, L. Chen, A.M. Beadle, S.S. Ferguson, A. Mezghrani, et al. 2006. ORL1 receptor-mediated internalization of N-type calcium channels. *Nat. Neurosci.* 9:31–40.
- Arundine, M., and M. Tymianski. 2004. Molecular mechanisms of glutamate-dependent neurodegeneration in ischemia and traumatic brain injury. *Cell. Mol. Life Sci.* 61:657–668.
- Brown, D.R. 2001. Prion and prejudice: normal protein and the synapse. *Trends Neurosci.* 24:85–90.
- Brown, D.R., J.W. Herms, B. Schmidt, and H.A. Kretzschmar. 1997. PrP and beta-amyloid fragments activate different neurotoxic mechanisms in cultured mouse cells. *Eur. J. Neurosci.* 9:1162–1169.
- Bueler, H., M. Fischer, Y. Lang, H. Bluethmann, H.P. Lipp, S.J. DeArmond, S.B. Prusiner, M. Aguet, and C. Weissmann. 1992. Normal development and behaviour of mice lacking the neuronal cell-surface PrP protein. *Nature.* 356:577–582.
- Carleton, A., P. Tremblay, J.D. Vincent, and P.M. Lledo. 2001. Dose-dependent, prion protein (PrP)-mediated facilitation of excitatory synaptic transmission in the mouse hippocampus. *Pflügers Arch.* 442:223–229.
- Colling, S.B., J. Collinge, and J.G. Jefferys. 1996. Hippocampal slices from prion protein null mice: disrupted Ca(2+)-activated K⁺ currents. *Neurosci. Lett.* 209:49–52.
- Colling, S.B., M. Khana, J. Collinge, and J.G. Jefferys. 1997. Mossy fibre reorganization in the hippocampus of prion protein null mice. *Brain Res.* 755:28–35.
- Collinge, J., M.A. Whittington, K.C. Sidle, C.J. Smith, M.S. Palmer, A.R. Clarke, and J.G. Jefferys. 1994. Prion protein is necessary for normal synaptic function. *Nature.* 370:295–297.
- Criado, J.R., M. Sanchez-Alavez, B. Conti, J.L. Giacchino, D.N. Wills, S.J. Henriksen, R. Race, J.C. Manson, B. Chessebro, and M.B. Oldstone. 2005. Mice devoid of prion protein have cognitive deficits that are rescued by reconstitution of PrP in neurons. *Neurobiol. Dis.* 19:255–265.
- Cull-Candy, S.G., and D.N. Leszkiewicz. 2004. Role of distinct NMDA receptor subtypes at central synapses. *Sci. STKE.* doi:10.1126/stke.2552004re16.
- Curtis, J., M. Errington, T. Bliss, K. Voss, and N. MacLeod. 2003. Age-dependent loss of PTP and LTP in the hippocampus of PrP-null mice. *Neurobiol. Dis.* 13:55–62.
- Dalva, M.B., A.C. McClelland, and M.S. Kayser. 2007. Cell adhesion molecules: signalling functions at the synapse. *Nat. Rev. Neurosci.* 8:206–220.
- DeArmond, S.J. 2004. Discovering the mechanisms of neurodegeneration in prion diseases. *Neurochem. Res.* 29:1979–1998.
- DeArmond, S.J., and S.B. Prusiner. 2003. Perspectives on prion biology, prion disease pathogenesis, and pharmacologic approaches to treatment. *Clin. Lab. Med.* 23:1–41.
- Dunah, A.W., J. Luo, Y.H. Wang, R.P. Yasuda, and B.B. Wolfe. 1998. Subunit composition of N-methyl-D-aspartate receptors in the central nervous system that contain the NR2D subunit. *Mol. Pharmacol.* 53:429–437.
- Fournier, J.G., F. Escaig-Haye, and V. Grigoriev. 2000. Ultrastructural localization of prion proteins: physiological and pathological implications. *Microsc. Res. Tech.* 50:76–88.
- Griffin, J.K., L.A. Terry, R. Jackman, M. Yousefi, and N.R. Cashman. 2007. Decreased cell surface prion protein in mouse models of prion disease. *Neuroreport.* 18:1–6.
- Herms, J.W., H.A. Kretzschmar, S. Titz, and B.U. Keller. 1995. Patch-clamp analysis of synaptic transmission to cerebellar purkinje cells of prion protein knockout mice. *Eur. J. Neurosci.* 7:2508–2512.
- Herms, J., T. Tings, S. Gall, A. Madlung, A. Giese, H. Siebert, P. Schurmann, O. Windl, N. Brose, and H. Kretzschmar. 1999. Evidence of presynaptic location and function of the prion protein. *J. Neurosci.* 19:8866–8875.
- Khosravani, H., C. Altier, G.W. Zamponi, and M.A. Colicos. 2005. The Arg473Cys-neuroligin-1 mutation modulates NMDA mediated synaptic transmission and receptor distribution in hippocampal neurons. *FEBS Lett.* 579:6587–6594.
- Lledo, P.M., P. Tremblay, S.J. DeArmond, S.B. Prusiner, and R.A. Nicoll. 1996. Mice deficient for prion protein exhibit normal neuronal excitability and synaptic transmission in the hippocampus. *Proc. Natl. Acad. Sci. USA.* 93:2403–2407.
- Maglio, L.E., M.F. Perez, V.R. Martins, R.R. Brentani, and O.A. Ramirez. 2004. Hippocampal synaptic plasticity in mice devoid of cellular prion protein. *Brain Res. Mol. Brain Res.* 131:58–64.
- Maglio, L.E., V.R. Martins, I. Izquierdo, and O.A. Ramirez. 2006. Role of cellular prion protein on LTP expression in aged mice. *Brain Res.* 1097:11–18.
- Mallucci, G.R., S. Ratté, E.A. Asante, J. Linehan, I. Gowland, J.G. Jefferys, and J. Collinge. 2002. Post-natal knockout of prion protein alters hippocampal CA1 properties, but does not result in neurodegeneration. *EMBO J.* 21:202–210.
- Mallucci, G.R., M.D. White, M. Farmer, A. Dickinson, H. Khatun, A.D. Powell, S. Brandner, J.G. Jefferys, and J. Collinge. 2007. Targeting cellular prion protein reverses early cognitive deficits and neurophysiological dysfunction in prion-infected mice. *Neuron.* 53:325–335.
- Manson, J.C., J. Hope, A.R. Clarke, A. Johnston, C. Black, and N. MacLeod. 1995. PrP gene dosage and long term potentiation. *Neurodegeneration.* 4:113–114.
- McLennan, N.F., P.M. Brennan, A. McNeill, I. Davies, A. Fotheringham, K.A. Rennison, D. Ritchie, F. Brannan, M.W. Head, J.W. Ironside, et al. 2004. Prion protein accumulation and neuroprotection in hypoxic brain damage. *Am. J. Pathol.* 165:227–235.
- Misra, C., S.G. Brickley, D.J. Wyllie, and S.G. Cull-Candy. 2000. Slow deactivation kinetics of NMDA receptors containing NR1 and NR2D subunits in rat cerebellar Purkinje cells. *J. Physiol.* 525:299–305.
- Mitsios, N., M. Saka, J. Krupinski, R. Pennucci, C. Sanfeliu, M. Miguel Turu, J. Gaffney, P. Kumar, S. Kumar, M. Sullivan, and M. Slevin. 2007. Cellular prion protein is increased in the plasma and peri-infarcted brain tissue after acute stroke. *J. Neurosci. Res.* 85:602–611.
- Mody, I., and J.F. MacDonald. 1995. NMDA receptor-dependent excitotoxicity: the role of intracellular Ca²⁺ release. *Trends Pharmacol. Sci.* 16:356–359.
- Muller, W.E., H. Ushijima, H.C. Schroder, J.M. Forrest, W.F. Schatton, P.G. Rytik, and M. Heffner-Lauk. 1993. Cytoprotective effect of NMDA receptor antagonists on prion protein (PrionSc)-induced toxicity in rat cortical cell cultures. *Eur. J. Pharmacol.* 246:261–267.
- Nazor, K.E., T. Seward, and G.C. Telling. 2007. Motor behavioral and neurological deficits in mice deficient for normal prion protein expression. *Biochim. Biophys. Acta.* 1772:645–653.
- Prusiner, S.B., M.R. Scott, S.J. DeArmond, and F.E. Cohen. 1998. Prion protein biology. *Cell.* 93:337–348.
- Rangel, A., F. Burgaya, R. Gavín, E. Soriano, A. Aguzzi, and J.A. Del Rio. 2007. Enhanced susceptibility of Prnp-deficient mice to kainate-induced seizures, neuronal apoptosis, and death: role of AMPA/kainate receptors. *J. Neurosci. Res.* 85:2741–2755.
- Rezaie, P., and P.L. Lantos. 2001. Microglia and the pathogenesis of spongiform encephalopathies. *Brain Res. Brain Res. Rev.* 35:55–72.
- Sakudo, A., T. Onodera, Y. Suganuma, T. Kobayashi, K. Saeki, and K. Ikuta. 2006. Recent advances in clarifying prion protein functions using knockout mice and derived cell lines. *Mini Rev. Med. Chem.* 6:589–601.
- Sales, N., K. Rodolfo, R. Hassig, B. Faucheu, L. Di Giambardino, and K.L. Moya. 1998. Cellular prion protein localization in rodent and primate brain. *Eur. J. Neurosci.* 10:2464–2471.
- Sassoon, J., M. Daniels, and D.R. Brown. 2004. Astrocytic regulation of NMDA receptor subunit composition modulates the toxicity of prion peptide PrP106–126. *Mol. Cell. Neurosci.* 25:181–191.

- Shyu, W.C., S.Z. Lin, M.F. Chiang, D.C. Ding, K.W. Li, S.F. Chen, H.I. Yang, and H. Li. 2005. Overexpression of PrPC by adenovirus-mediated gene targeting reduces ischemic injury in a stroke rat model. *J. Neurosci.* 25:8967–8977.
- Spudich, A., R. Frigg, E. Kilic, U. Kilic, B. Oesch, A. Raeber, C.L. Bassetti, and D.M. Hermann. 2005. Aggravation of ischemic brain injury by prion protein deficiency: role of ERK-1/-2 and STAT-1. *Neurobiol. Dis.* 20:442–449.
- Steele, A.D., S. Lindquist, and A. Aguzzi. 2007. The prion protein knockout mouse: a phenotype under challenge. *Prion.* 1:83–93.
- Thompson, C.L., D.L. Drewery, H.D. Atkins, F.A. Stephenson, and P.L. Chazot. 2002. Immunohistochemical localization of N-methyl-D-aspartate receptor subunits in the adult murine hippocampal formation: evidence for a unique role of the NR2D subunit. *Brain Res. Mol. Brain Res.* 102:55–61.
- Vassallo, N., and J. Herms. 2003. Cellular prion protein function in copper homeostasis and redox signalling at the synapse. *J. Neurochem.* 86:538–544.
- Vicini, S., J.F. Wang, J.H. Li, W.J. Zhu, Y.H. Wang, J.H. Luo, B.B. Wolfe, and D.R. Grayson. 1998. Functional and pharmacological differences between recombinant N-methyl-D-aspartate receptors. *J. Neurophysiol.* 79:555–566.
- Walz, R., O.B. Amaral, I.C. Rockenbach, R. Roesler, I. Izquierdo, E.A. Cavalheiro, V.R. Martins, and R.R. Brentani. 1999. Increased sensitivity to seizures in mice lacking cellular prion protein. *Epilepsia.* 40:1679–1682.
- Wang, Y.T., and M.W. Salter. 1994. Regulation of NMDA receptors by tyrosine kinases and phosphatases. *Nature.* 369:233–235.
- Weise, J., O. Crome, R. Sandau, W. Schulz-Schaeffer, M. Bahr, and I. Zerr. 2004. Upregulation of cellular prion protein (PrP^c) after focal cerebral ischemia and influence of lesion severity. *Neurosci. Lett.* 372:146–150.
- Weise, J., R. Sandau, S. Schwarting, O. Crome, A. Wrede, W. Schulz-Schaeffer, I. Zerr, and M. Bahr. 2006. Deletion of cellular prion protein results in reduced Akt activation, enhanced postischemic caspase-3 activation, and exacerbation of ischemic brain injury. *Stroke.* 37:1296–1300.